

# Experimental–numerical investigation on the seismic behaviour of moment-resisting timber frames with densified veneer woodreinforced timber joints and expanded tube fasteners

**Citation for published version (APA):**

van Bakel, R. H. B., Rinaldi, G., Leijten, A. J. M., & Fragiacomio, M. (2017). Experimental–numerical investigation on the seismic behaviour of moment-resisting timber frames with densified veneer woodreinforced timber joints and expanded tube fasteners. *Earthquake Engineering & Structural Dynamics*, 46(8), 1307-1324. <https://doi.org/10.1002/eqe.2857>

**DOI:**

[10.1002/eqe.2857](https://doi.org/10.1002/eqe.2857)

**Document status and date:**

Published: 10/07/2017

**Document Version:**

Accepted manuscript including changes made at the peer-review stage

**Please check the document version of this publication:**

- A submitted manuscript is the version of the article upon submission and before peer-review. There can be important differences between the submitted version and the official published version of record. People interested in the research are advised to contact the author for the final version of the publication, or visit the DOI to the publisher's website.
- The final author version and the galley proof are versions of the publication after peer review.
- The final published version features the final layout of the paper including the volume, issue and page numbers.

[Link to publication](#)

**General rights**

Copyright and moral rights for the publications made accessible in the public portal are retained by the authors and/or other copyright owners and it is a condition of accessing publications that users recognise and abide by the legal requirements associated with these rights.

- Users may download and print one copy of any publication from the public portal for the purpose of private study or research.
- You may not further distribute the material or use it for any profit-making activity or commercial gain
- You may freely distribute the URL identifying the publication in the public portal.

If the publication is distributed under the terms of Article 25fa of the Dutch Copyright Act, indicated by the “Taverne” license above, please follow below link for the End User Agreement:

[www.tue.nl/taverne](http://www.tue.nl/taverne)

**Take down policy**

If you believe that this document breaches copyright please contact us at:

[openaccess@tue.nl](mailto:openaccess@tue.nl)

providing details and we will investigate your claim.

# Experimental–numerical investigation on the seismic behaviour of moment-resisting timber frames with densified veneer wood-reinforced timber joints and expanded tube fasteners

R. van Bakel<sup>1</sup>, G. Rinaldin<sup>2</sup>, A. J. M. Leijten<sup>1,\*</sup> and M. Fragiaco<sup>3</sup>

<sup>1</sup>*Department of Built Environment, Eindhoven University of Technology, Eindhoven, The Netherlands*

<sup>2</sup>*Department of Architecture, Design and Urban Planning, University of Sassari, Sassari, Italy*

<sup>3</sup>*Department of Civil, Construction–Architectural and Environmental Engineering, University of L'Aquila, L'Aquila, Italy*

## SUMMARY

This paper investigates the seismic behaviour of moment-resisting timber frames with beam-column joints fastened with expanded tubes and reinforced with densified veneer wood. Laboratory experiments are carried out on single joints to investigate the cyclic behaviour and, more specifically, the impairment of strength, the ductility ratio and the equivalent viscous damping ratio. A phenomenological numerical model is proposed, where the beams and columns are schematized using linear-elastic beam elements, and the joints with non-linear hysteretic spring calibrated on the results of the experimental tests. The model is used to analyse some representative moment-transmitting structures characterised by different number of bays and storeys. After an estimation of the lateral load-carrying capacity using a pushover analysis, the numerical model is used to estimate the behaviour factor. An incremental dynamic analysis is performed using a set of accelerograms spectrum consistent with a chosen design spectrum. The analyses lead to an estimation of the behaviour factor of 3 and 6 for a portal frame and a five-storey, three-bay frame, respectively, which confirms the highly dissipative behaviour of this kind of moment connection. Copyright © 2017 John Wiley & Sons, Ltd.

Received 15 June 2016; Revised 8 November 2016; Accepted 14 November 2016

KEY WORDS: densified veneer wood; timber frame; tube fasteners; non-linear springs; behaviour factor; moment-resisting frame

## 1. INTRODUCTION

Timber structures represent nowadays a suitable alternative to concrete and steel, even for medium-rise to high-rise buildings and for earthquake-prone areas. For many years, a great research effort has been made to estimate the dissipative capacity and thus the seismic vulnerability of different timber systems, including light-frame construction, cross-laminated systems and moment-resisting frames, to list the most common ones. Dowels or bolts are generally used as fasteners in timber connections, the load-carrying capacity of which is calculated using the Johansen theory [1]. However, structural design in seismic regions requires special focus on ductility and dissipation of energy in addition to strength. Previous studies performed by Leijten *et al.* [2–5] showed that using metal tubes fasteners instead of dowels in combination with reinforcement of the timber connections with densified veneer wood (DVW) beech plywood results in mechanical properties superior to many other existing timber

\*Correspondence to: A. J. M. Leijten, Department of Built Environment, Eindhoven University of Technology, Eindhoven, The Netherlands.  
E-mail: A.J.M.Leijten@tue.nl

connections, Figure 1. The DVW sheets are separately glued to each timber member using an epoxy resin adhesive Aerodux 185 with a powder hardener (HRP 155).

Their purpose is to avoid premature failure of the timber caused by the embedment stresses at the interface with the fasteners. The embedment forces are resisted by the DVW and distributed over a large glued surface. The DVW plywood sheets consist of 1-mm-thick veneers that are layered crosswise. Tests presented in [2] have shown this layup results in isotropic embedment properties. The reinforcement of the connection combined with the use of mild steel tube fasteners results in a ductile behaviour in static tests [4, 5]. During assembly, the tubes are expanded in the oversized pre-drilled holes with a hydraulic jack to remove the hole clearance. This assembly process increases the initial stiffness and ensures immediate load take-up. Previous research on reversed-cyclic behaviour of the DVW connections with expanded tube fasteners showed a ductility ratio and ultimate rotation significantly higher than using traditional dowel-type fasteners as shown in [6]. Past investigations carried out on dowel-type connections mainly focused on the estimation of the effective load-carrying capacity. Jorissen [7] experimentally studied multiple dowel-type connections and discussed a load distribution model. Blass *et al.* [8] investigated a modification of the Johansen's yield theory. Uibel and Blass extended such a study to solid wood (cross-laminated) panels [9] and Dias *et al.* to timber-concrete connections [10]. Despite the numerous research works on this topic, none of the above is related to the expanded tube fastener connections.

In this paper, experiments on DVW connections are presented and critically discussed. Fully reversed-cyclic tests are carried out and used to calibrate a previously developed numerical model for seismic investigations of timber structures [11, 12]. Different planar moment-transmitting frames have then been analysed via non-linear static (pushover) and non-linear dynamic (time-history) analyses. The behaviour factor  $q$  is then estimated as a ratio between the peak ground acceleration (PGA) needed for the first connection to attain the ultimate rotation and the PGA leading to the plasticization of the first connection, as already carried out in [14, 15].

## 2. LABORATORY TESTS

The purpose of the experimental tests was to characterise the cyclic behaviour of the connection under fully reversal loading with a particular focus on features such as impairment of strength and stiffness degradation. The ductility values and the equivalent viscous damping ratio (EVDR) were determined in accordance with EN 12512 [16]. The loading protocol prescribed by this standard was followed, which considers the displacement associated with the onset of yielding as a starting point. The yield displacement was estimated using the test protocol of EN 26891 [17]. Once the yield displacement was known, the yield rotation could be calculated.

### 2.1. Test series

Three different test series with T-shaped specimens had been tested, Series P0, P1 and P2. The strength class of the laminations used for the production of the glued laminated timber members was C24

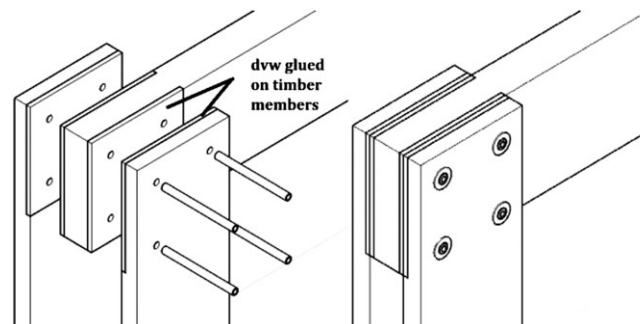


Figure 1. Densified veneer wood (DVW) reinforced timber connection with expanded tube fasteners before (left) and after (right) the assembly.


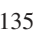
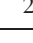
according to EN338, which corresponds to a characteristic bending strength of 24 N/mm<sup>2</sup>. The wood species was Norway Spruce. The mean wood density was 451 kg/m<sup>3</sup> with a mean moisture content of 11%. The T-shaped specimens consisted of two horizontal side members and one vertical middle member. The cross-sectional dimensions of the glued laminated middle and side members were the same. Details about the test series are presented in Table 1. The 18- and 35-mm-diameter tubes of mild steel had wall thicknesses of 2.35 and 3.25 mm, respectively. The test series P0 and P2 consisted of four tubes located at the connection corners at 120- and 248-mm distance from the connection centre, respectively, as shown in Figure 2.

The edge and end distances were 3.5 times the tube diameter. The connection area was 300 by 300 mm for P0, 400 by 400 mm for P1 and 600 by 600 mm for P2 Series. The connection of the test Series P1 had six 18-mm-diameter tubes altogether: four at the corners and two in between.

Series P1 was tested to check the consistency of the results when trying to predict its behaviour using the results of Series P0. Series P2 had a fastener layout comparable to Series P0. However, the diameter of the tubes was 35 mm, and the timber members were larger than Series P0. The distance between the centre of the connection and the point of load introduction was 2400 mm for all test specimens. The length of all horizontal side members was 3000 mm with the connection placed in the middle. To prevent splitting of the vertical member at the point of load application, the loading area was reinforced by gluing two sheets of 18-mm plywood to each face, see Figure 3.

The DVW reinforcement, supplied by the company Lignostone International, was decisive for the mechanical properties of the connection, as the previous research carried out by Leijten [2] showed. The density of the DVW plywood was about 1200 kg/m<sup>3</sup>. DVW is intended to be used for indoor climatic conditions as substantial swelling in thickness occurs when directly exposed to water (rain). To prevent undesirable swelling for short periods, the edges can be sealed. The DVW reinforcement was glued to each face of the middle member and the corresponding face of the side members, covering in this way the whole connection area. The DVW thicknesses are listed in the last column of Table 1. The adhesive used to glue the DVW to the timber members was a liquid phenol resorcinol Aerodux 185, mixed with the powder hardener HRP 155. Prior to the gluing process, the DVW sheets were sanded. The glue line pressure was achieved by applying screws in pre-drilled holes in each DVW sheet. The loads required to expand the metal tubes were 80 and 160 kN for the 18-m and 35-mm-diameter tube, respectively. More details about the oversized holes and over-length of the tubes are given in Leijten [2].

Table I. Dimensions and parameters of each test series.

Test series	Number of specimens	Tube diameter [mm]	Number of tubes	Cross-section dimension Middle and side member [mm × mm]	Distance to connection centre R [mm]	DVW thickness [mm]
P0	3	18	4	45 × 300	120 	12
P1	1	18	6	80 × 400	135/191 	15
P2	3	35	4	80 × 600	248 	18

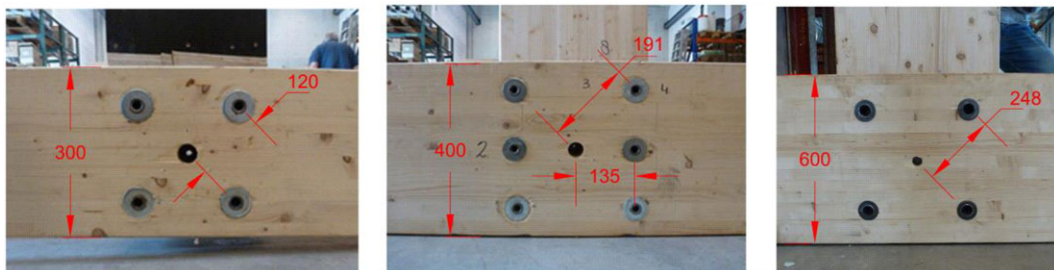


Figure 2. Test series P0 (left), P1 (middle) and P2 (right), units in millimetres.

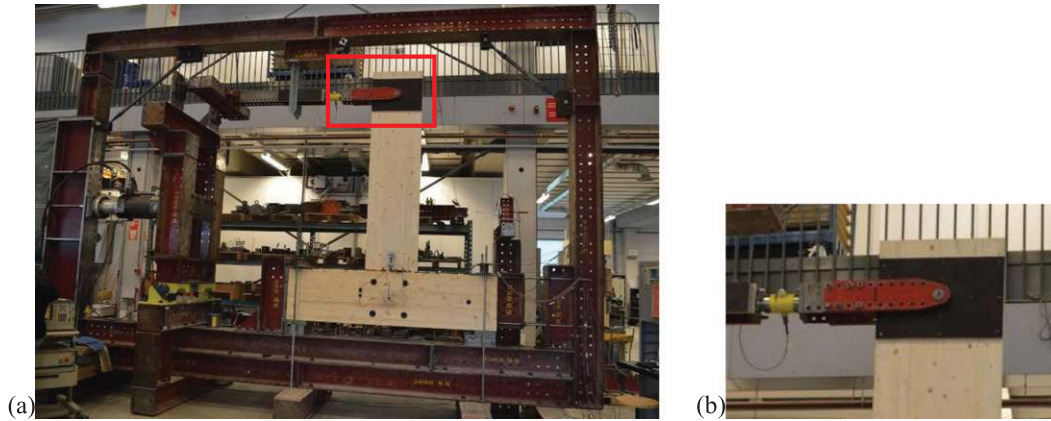


Figure 3. Photo of the test rig with specimen series P2 (left) and detail of the plywood sheet at the loading point (right).

## 2.2. Test setup

The test specimens were subjected to a horizontal quasi-static load as prescribed by EN 12512 [16]. The test rig is displayed in Figure 3. Because the stroke length of the actuator was too short for the intended deflection of the specimens at the load introduction, a lever arm was used to increase the maximum horizontal displacement to 400 mm. The load introduction and the end of the lever arm were placed as high as possible, to keep the shear force in the connection as low as possible. The top end of the lever arm was connected to the T-shape test specimen by a horizontal steel member hinged on both ends. The horizontal movement and vertical uplift of the test specimen were prevented by end supports. The lower pivot point of the lever arm corresponded to the centre line of the connection. The end of the lever arm corresponded to the load introduction of the specimen ensuring a horizontal load application throughout the test procedure. The actuator was connected with hinges to the test rig and the lever arm. The displacement of the hydraulic actuator was controlled by an external computer, where a custom-made programme followed the prescribed displacement history of EN 12512 [16]. The prescribed displacements at the load introduction were monitored by a linear variable displacement transducer (LVDT). All the other displacements were also measured using LVDTs. Out of plane deformations were prevented by a lateral stability element. The applied force was measured by a load cell close to the load introduction, see Figure 4.

To perform the test accurately, the relative rotation and translation of the horizontal members with respect to the vertical middle timber member were measured at the connection centre using a purposely built rotation and displacement measurement (RDM) apparatus as shown in Figure 5. The RDM was mounted at the centre of the connection area, where the vertical and horizontal centre lines intersect. The centre line of the middle (vertical) timber member was taken as the  $y$ -axis and the centre of the longitudinal (horizontal) timber side member as the  $x$ -axis. The RDM consisted of two plexiglas sheets, a square and a triangle one, and three LVDTs (labelled A, B and C in Figure 5). The square plexiglas sheet was screwed to the side member near the centre of the connection area. The triangular plexiglas sheet was connected to the centre of the middle timber member using a 8-mm-diameter threaded steel rod. This rod was fixed with two nuts to the DVW of the middle member. In order to fix the steel rod to the middle member, a hole was drilled in the side members big enough to allow translation movements of the middle member relative to the side member.

The LVDTs were all fixed to the square sheet and measured the rotation of the triangle sheet. The LVDTs labelled C and B were parallel to and aligned with the  $x$ -axis and  $y$ -axis, respectively, and recorded the corresponding translations  $w_x$  and  $w_y$ . Both LVDTs took the measurement at the edges of the triangle sheet 50 mm away from the intersection of the  $x$  and  $y$  axes denoted with  $M$ . Only LVDT A was fixed 150 mm from the centre  $M$  and was parallel to LVDT B. Using the data

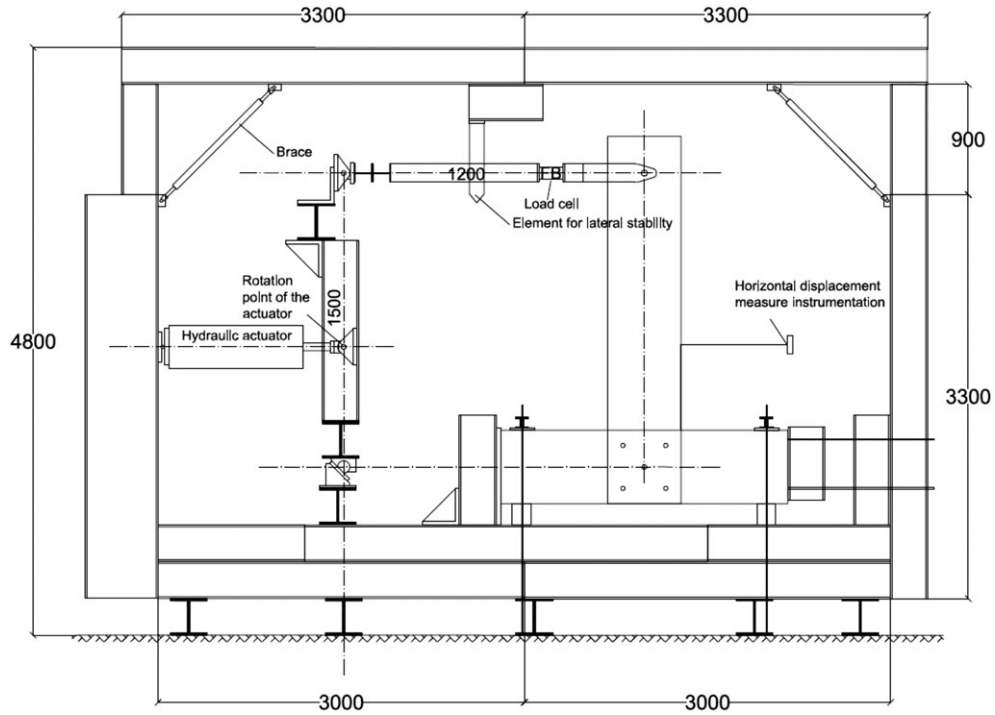


Figure 4. Schematic of the test setup, units in millimetres.

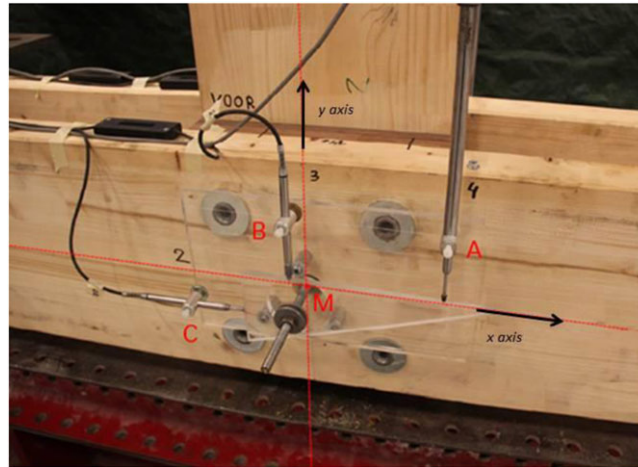


Figure 5. Measurement of relative rotation and displacement in the joint.

recorded by LVDT, A and B allowed the determination of the relative rotation of side and middle member with Eqn (1), with  $w_B$  and  $w_C$  signifying the displacements recorded by LVDTs B and C.

$$\phi = \tan^{-1} \left( \frac{w_A - w_B}{150} \right) \quad (1)$$

The displacements  $w_{x,M}$  and  $w_{y,M}$  at the connection centre M in x and y directions were affected by the rotation and require adjustment using Eqn (2).

$$\begin{aligned} w_{x,M} &= \cos(2\phi)w_B + 0,5 \sin(2\phi)w_C + 50(1 - \cos\phi)(\cos\phi + \sin\phi) \\ w_{y,M} &= \cos(2\phi)w_C + 0,5 \sin(2\phi)w_B + 50(\cos\phi - 1)(\sin\phi - \cos\phi) \end{aligned} \quad (2)$$

The equations can easily be derived using the geometry of the Plexiglas sheets and the positions of the LVDT's as given in Figure 6.

### 3. TEST RESULTS

The load procedure according to EN 12512 was based on the displacement associated with the onset of yielding. Preliminary shear tests carried out in accordance with EN 12512 on single-tube fasteners showed that the yield displacement were 1.00 and 0.98 mm for the 18- and 35-mm-diameter tube, respectively. The corresponding shear forces were 47 and 109 kN per tube. Using this information, the onset of yield rotation and the corresponding displacement at the load introduction point of the T-shaped test specimen could be estimated. For test Series P0 and P2, the estimated rotation at the onset of yielding was 0.0083 rad for the 18-mm-diameter tube and 0.0040 rad for the 35-mm-diameter tube. The bending moments corresponding to these rotations were 22.6 and 107.9 kNm, respectively. Using the data of similar tests carried out by Leijten [2] results in 0.0085 and 0.0045 rad for the onset of yield rotation with 24.7 and 123.8 kNm as bending moment, respectively. The expected maximum deflection at the load introduction point was 400 mm. Based on the preliminary tests, tube failure was expected at a bending moment of 37.5 kNm and corresponding to a rotation of 0.11 rad for the 18-mm-diameter tube. For the 35-mm-diameter tube, the values were 185 kNm and the rotation 0.067 rad. These values are summarised in Table 2.

Although the test specimens were designed not to fail in the timber part prior to the failure of the tube fastener, nevertheless it happened once for a specimen of the P0 test Series where the middle member failed in bending prematurely. This failure occurred in a finger joint of the outer lamination loaded in tension. In practice, timber failure is prevented by using the 5% lower characteristic strength values when designing the timber parts. Failure of the connection was defined when the

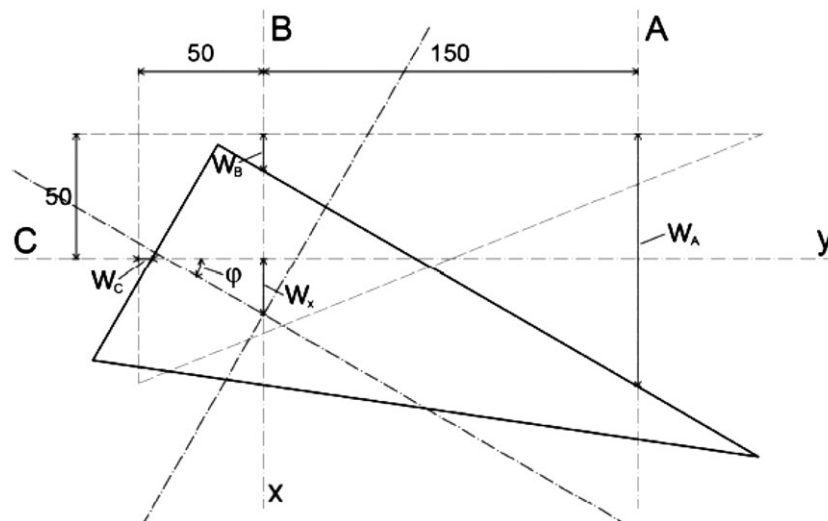


Figure 6. Geometry of the MDR device and locations of the linear variable displacement transducer a, b and c.

Table II. Yield displacements and rotations, and corresponding shear forces and moments of each test series.

Test specimen	Yield displacement [mm]	Yield force [kN]	$R_{\text{tube}}^{\dagger}$ [mm]	Yield rotation [rad]	Yield moment [kNm]
18-mm tube	1.02	51.42	120.21	0.0083	22.6
35-mm tube	1.12	125.10	247.48	0.0040	107.9

<sup>†</sup>The distance from the centre of the tube fasteners to the geometrical centre of the connection.

impairment of strength in subsequent load cycles dropped more than 20%. Figure 7 shows the representative hysteresis curves of test specimens P0-03 and P2-02. The hysteresis curves are based on the average of the rotations recorded by the RDM on either side of the connection. Figure 8 shows the history of the relative displacement recorded in the middle member in the  $x$  and  $y$  directions with respect to the side member for test specimen P2-02. The vertical displacement along the  $y$ -axis did not exceed 1.2 mm and showed that the influence of the vertical shear load given by the self-weight of the specimen and by the load application beam was small. The gradual sagging of the average this curve over time was on average 0.6 mm. The horizontal displacement along the  $x$ -axis attained the maximum value of 5 mm and represents the effect of the horizontal shear load that was obviously much more significant than the effect of the self-weight.

The moment–rotation curves of Figure 7 can be easily transformed into a force–displacement curve using simple statics and ignoring the minor influence by the vertical and horizontal shear load. In this case, the total bending moment is the resultant of the moments of the shear forces at the two shear planes of each tube. Such shear forces were assumed as proportional to the distance of the tube fastener from the rotation centre  $M$ . The result is displayed in Figure 9 as force per shear plane.

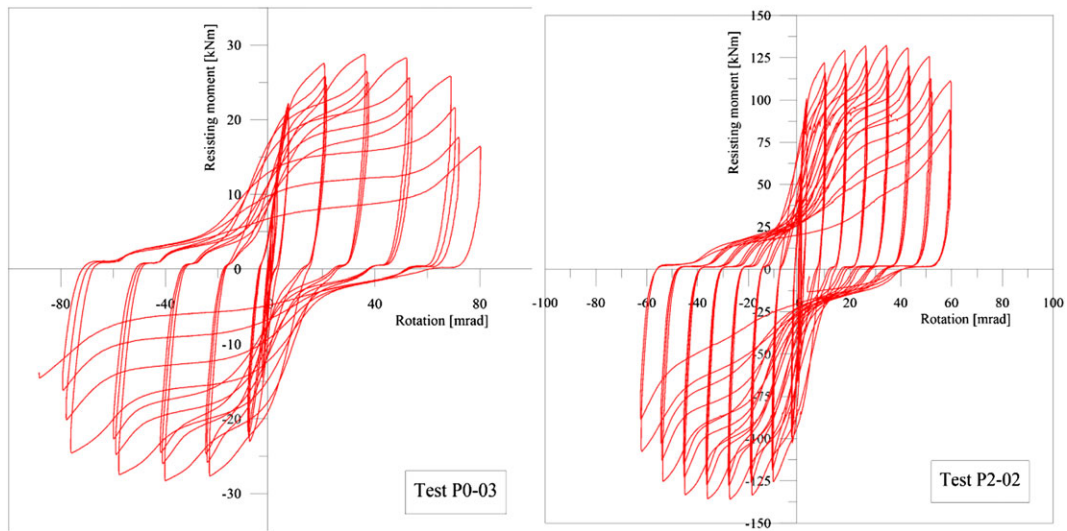


Figure 7. Hysteresis curves of Series P0 specimen, 18-mm-diameter tube (left) and Series P2 specimen, 35-mm-diameter tube (right).

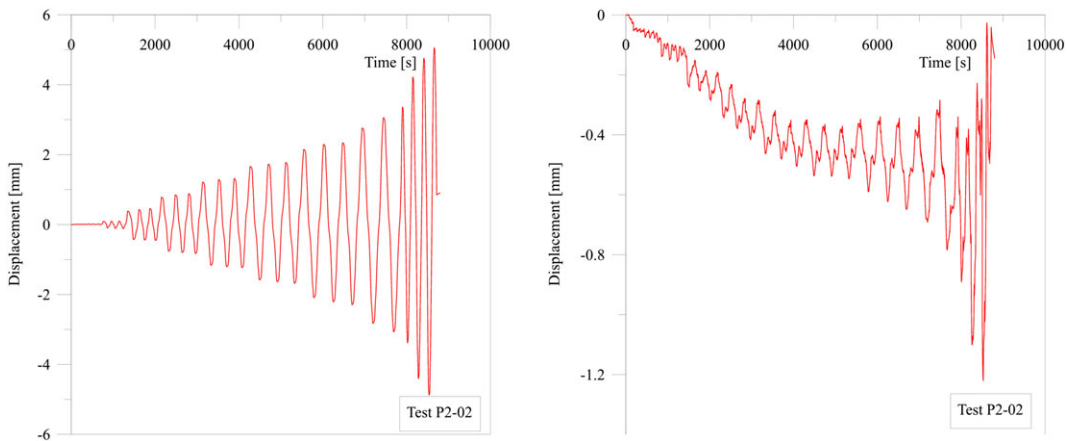


Figure 8. History of recorded relative vertical  $y$ -displacement (left) and horizontal  $x$ -displacement (right) at the connection centre. P2, 35-mm tube (right).



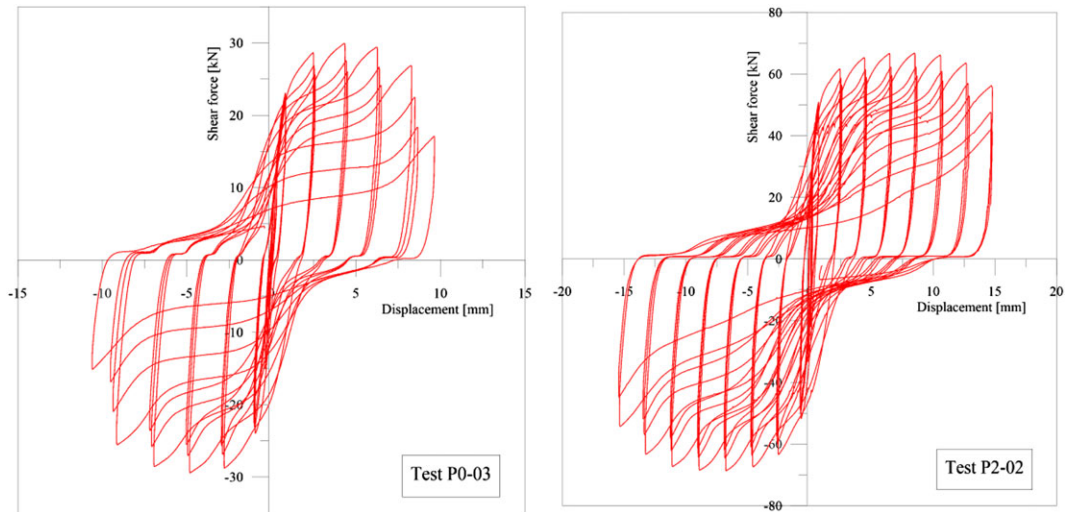


Figure 9. Force–displacement curves per shear plane for the Series P0, 18-mm tube (left) and Series P2, 35-mm tube (right). The strength and stiffness properties experimentally measured by Leijten in single-shear static tests [2] are shown in Table 3. All strength and stiffness properties refer to single-tube and single-shear plane.

Table III. Characteristic strength and mean stiffness for design calculation purposes.

Tube diameter [mm]	Min. DVW thickness [mm]	ULS strength <sup>†</sup> [kN]	SLS stiffness <sup>‡</sup> [kN/mm]	ULS stiffness <sup>#</sup> [kN/mm]
18	12	35	30	15
35	18	96	65	20

<sup>†</sup>Characteristic strength (5% fractile) per shear plane per tube: for double tubes add 15%.

<sup>‡</sup>Mean stiffness per shear plane per tube for SLS design: for double tubes add 15%.

<sup>#</sup>Mean stiffness per shear plane per tube for ULS design: for double tubes double the value.

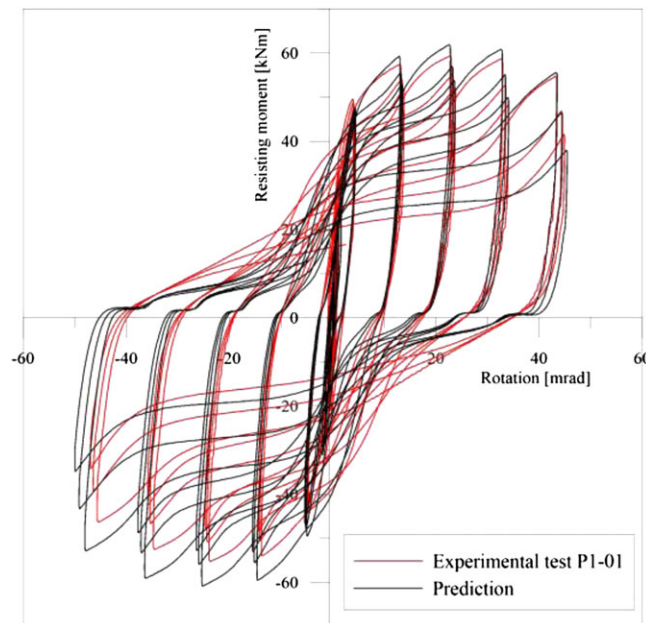


Figure 10. Predicted and recorded hysteresis loops of test Series P1-01.

To demonstrate the consistent behaviour of the tube connection, the force–displacement records of test Series P0 were used to predict the moment–rotation curves of test Series P1-01. This test series had not only tube fasteners at the four corners of the connection area but also two tubes located halfway as shown in Figure 2. Assuming the shear force in the tube is proportional to the distance of the fastener from the centre of the connection area, the result of this transformation is given in Figure 10 (blue solid curve) and compared with the actual recorded test data (red solid curve). A final difference on total energy less than 16% demonstrated that the hysteretic behaviour of connections with different tube fastener patterns can be predicted from the hysteretic behaviour of a single-tube fastener.

The energy dissipation of a connection is an important property of seismic-resistant joints, which is measured by the EVDR according to the European Standard [19] by using the hysteresis curves. This non-dimensional parameter is measured as the ratio between the dissipated energy in half cycle and the available potential energy multiplied by  $2\pi$ . The EVDR values of the expanded tube fastener connection is calculated and compared with other examples of ductile connections developed by Kasal [28] and Schreyer [29]. Kasal tested connections reinforced with DVW using solid dowels, whereas Schreyer tested steel-to-timber connections with slender dowels and without reinforcement. Figure 11 plots the EVDR values of the different connections versus the loop number. The difference among the energy dissipation using DVW-reinforced connections with expanded tubes or with normal dowels (Schreyer [29]) is remarkable. The connections with slender dowels show a lower dissipative behaviour, as displayed in Figure 11. The energy dissipation clearly increases when the tubes enter the plastic deformation phase that corresponds to loop number 20–24. The DVW-reinforced tube connections even reach EVDR values higher than 0.3 at some deformation steps.

In the European design standard EN1998-1 [13] known as Eurocode 8, three ductility classes are introduced: low (L), medium (M) and high (H). A medium class system requires dissipative joints with a ductility ratio  $>4$ , while an H-class structure requires joints with ductility levels  $>6$  without more than 20% reduction of resistance in subsequent load cycles. The impairment of strength of specimen P0-02 exceeds the 20% at the 7th triple displacement cycle. This makes the connection belong to ductility class H, having attained a ductility ratio of 6.6 at the sixth triplet displacement cycle with an impairment of strength of 19.8%. For the specimens with the 35-mm-diameter tube, failure was governed by the impairment of strength of 18.9% at the 10th triple displacement cycle resulting in a ductility ratio of 14.7.

To compare the reported characteristic static and cyclic strength, the test results of specimens P0 and P2 have to be modified. The characteristic cyclic strength is determined according to EN 14358 [19].

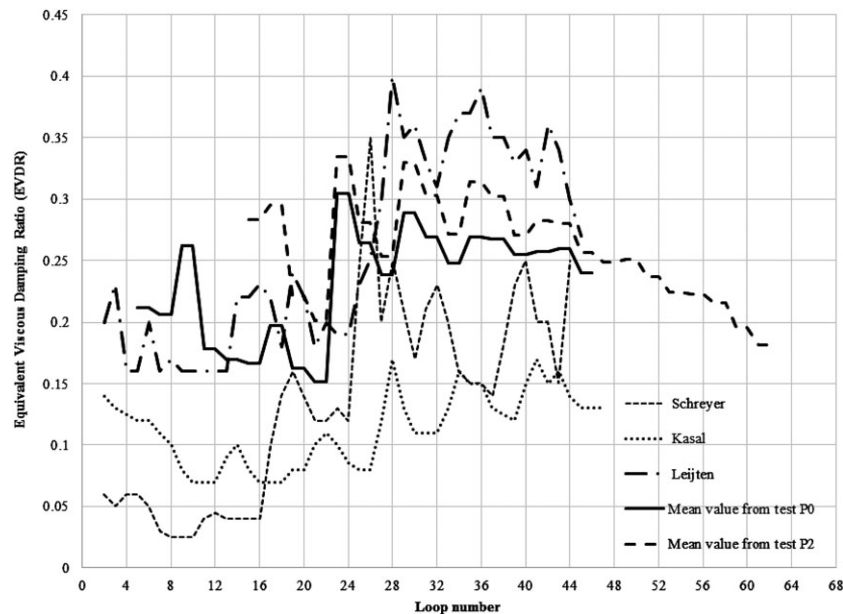


Figure 11. Comparison of equivalent viscous damping ratios for different ductile connections.

Table IV. Mean and characteristic strength.

Test specimen	Mean strength [kN]	Characteristic strength [kN]
P0	27.51	25.60
P2	66.18	57.15

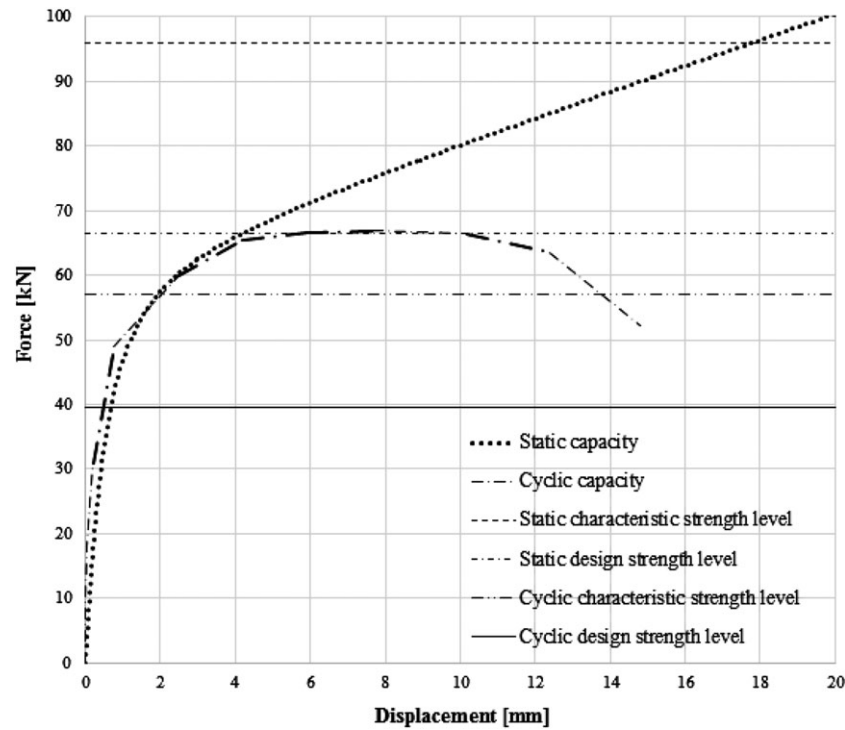


Figure 12. Static and cyclic (first backbone) shear force–slip curve of one tube per shear plane.

This European Standard described the calculation of characteristic 5-percentile values and acceptance criteria for a sample. In Table 4, the mean value and characteristic strength are presented.

Figure 12 shows the force–displacement curves for static and cyclic (backbone curves) loading. The levels of the characteristic static and cyclic strength are also indicated. To obtain the design values according to Eurocode 5, the characteristic strengths are multiplied by appropriate values of  $k_{\text{mod}}$  accounting for load duration and moisture effect and divided by the partial material factor. Different values apply when design is made corresponding to Eurocode 8 [13].

The rotational stiffness of the connection,  $k_{\phi}$  is simply calculated with Eqn (3) (Figure 13).

$$k_{\phi} = n s \sum_n k_{\text{tr}} R^2 \quad (3)$$

Table 5 compares the results of Eqn (3) with the experimental results obtained from the RDM data. The differences are below 4%, demonstrating that the connection behaviour can be predicted using the proposed approach.

#### 4. NUMERICAL MODELLING

The numerical approach proposed by Rinaldin *et al.* [11] has been used to model the investigated connection. The model consists of a phenomenological non-linear spring with a slip-type hysteresis law, and it has been successfully used to model connections in several types of timber systems such

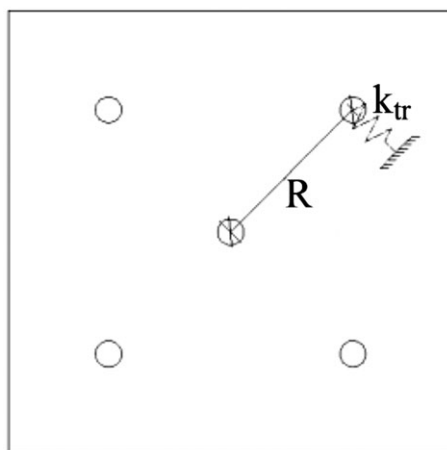


Figure 13. Schematics used to calculate the joint rotational stiffness with  $n$  number of tubes;  $s$  number of shear planes (two in this case);  $k_{tr}$  translational stiffness of a tube;  $R$  distance between the tube location and the rotation centre.

Table V. Rotational stiffnesses.

Tube diameter [mm]	Shear stiffness from Table 3 [kN/mm]	Distance between the tube and rotation centre [mm]	Rotational stiffness [kNm/rad]	Rotational stiffness from RDM data [kNm/rad]	Difference in rotational stiffness [%]
18	30	120.2	3468	3352	3.5
35	65	247.5	31 853	30 634	4.0

RDM, rotation and displacement measurement.

as cross-laminated [30], log-house [31] and light-frame structures [32], and also to model non-linear rotational joints [14, 15]. The nature of this modelling approach allows the user to perform non-linear static and dynamic analyses with a limited computational effort, making it suitable for incremental dynamic analyses (IDA). Figure 14(a) depicts the piecewise law implemented in the model, composed by a tri-linear backbone curve and different unloading and reloading paths.

Stiffness and strength degradations are taken into account; further information on their formulation can be found in [11]. The degradation parameters have been obtained from an iterative calibration process, presented later on.

In this paper, such model has been employed for representing the entire dowel-type joint in the moment  $M$ -rotation  $\varphi$  plane, as schematically depicted in Figure 14(b). Hence, the frames have continuous linear-elastic beams and columns, which have been connected through flexural springs with non-linear hysteretic behaviour.

## 5. SPRING CALIBRATION

The calibration of the rotational springs has been performed for each cyclic test presented in this paper. A set of 16 input parameters is required. Such process has been carried out with a purposely developed software [18] through two steps: (i) calibration of the backbone curve according to the EN 12512 regulation [16] and (ii) iterative calibration of the parameters defining the hysteresis cycles.

At the first step, once implemented the experimental moment-rotation curve of Figure 15(a), the software automatically determines the elastic and the hardening branches of the backbone curve according to EN 12512 [16]. After that, a further softening branch is set starting from the point of maximum strength and the related displacement, and assuming as final point that where the strength loss, during repeated load cycles, exceeds 20% of the peak strength.

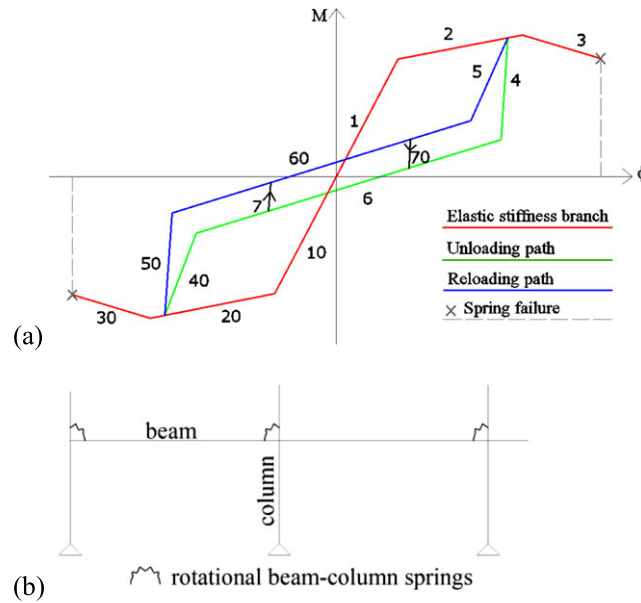


Figure 14. Symmetric moment–rotation hysteresis law for the rotational springs, with branch numbers (a) and frame schematization with rotational springs (b).

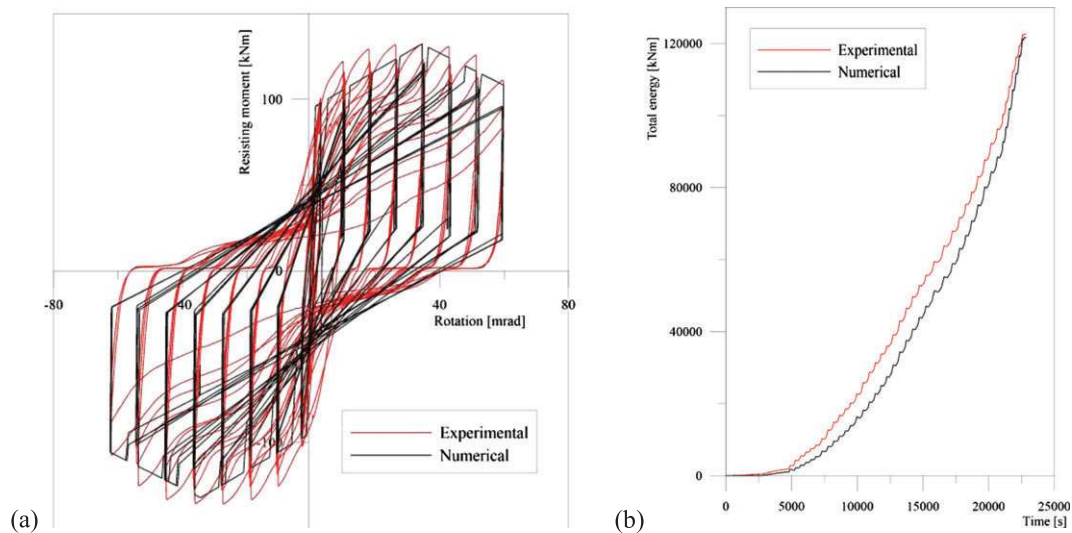


Figure 15. Experimental–numerical comparisons of resisting moment versus rotation curves (left) and time-histories of total energy (right) for the joint test P2-02.

In the second step, the cyclic parameters are set: initially, the software suggests some values, which can then be refined by the user or through an automatic optimization process [18]. The process ends when the final value of total experimental energy calculated by integration of the experimental curves implemented and the total energy given by the model approximation differs from less than 5%, which was considered a satisfactory value in previous works [11, 12, 15]. As an additional constraint in the described iterative procedure, the difference between the numerical moment and the corresponding experimental value at the same rotation is minimised, in this way limiting the sets of parameters that can be obtained as a result. Figure 15 shows the calibration used for the test P2-02 and a comparison between experimental and numerical total energy time-histories (Figure 16).

The obtained parameters, listed in Table 6, have been used in the subsequent dynamic analyses. The first five parameters are related to the definition of stiffnesses ( $K_i$ ) and strength ( $F_i$ ) associated with the

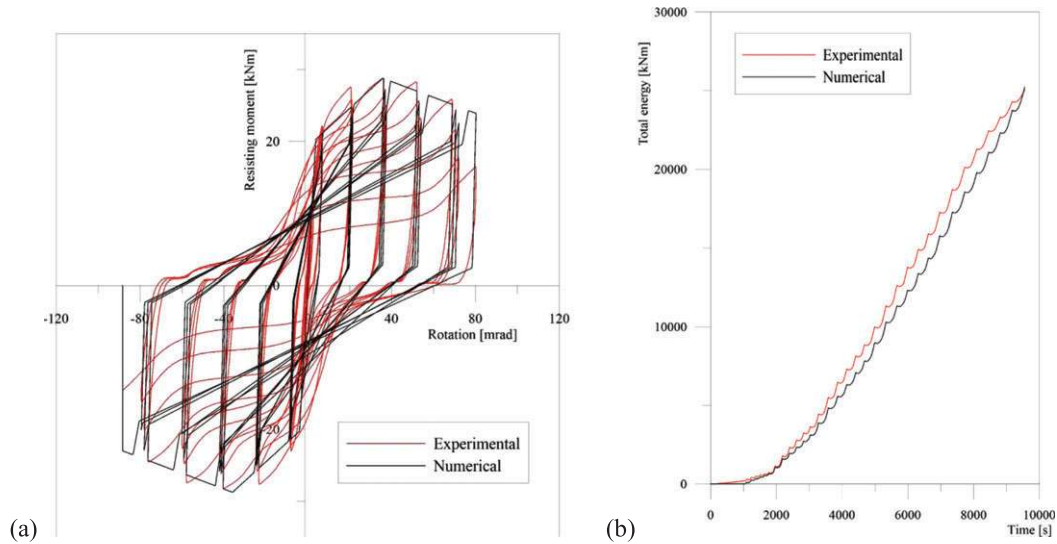


Figure 16. Experimental–numerical comparisons of resisting moment versus rotation curves (left) and time-histories of total energy (right) for the joint test P0-03.

Table VI. Parameters obtained from model calibration to tests P2-02 and P0-03.

Parameter	P0-03	P2-02
$K_{el}$ [kNm]	5.204	70.028
$F_y$ [kNm]	20.288	95.992
$K_{1pl}$ [kNm]	0.266	1.098
$F_{max}$ [kNm]	28.78	132.21
$K_{2pl}$ [kNm]	-0.11	-0.941
$k_{unl}$	2.318	3.265
$R_C$	0.204	0.11
$S_C$	0.9	0.8
$\phi_{ult}$ [mrad]	88.276	62.459
$\alpha$	1	1
$\gamma$	0.000505	0.000505
$c_5$	0.5	0.5
Total energy diff. (%)	-0.05	-0.78

backbone curve, while  $\phi_{ult}$  signifies the ultimate rotation of the spring. The factors  $k_{unl}$  and  $c_5$  determine the stiffnesses of branches 4/50 and 5/40, respectively, while  $R_C$  and  $S_C$  set the unloading and reloading ratio from and to the backbone curve, respectively. Finally,  $\alpha$  and  $\gamma$  are the strength degradation parameters [11].

## 6. Q-FACTOR ESTIMATION OF FRAME ASSEMBLIES

In the past work of Wrzesniak *et al.* [15], the behaviour factor  $q$  was evaluated on plane frame structures with expanded tube fasteners through IDA, already used by Ceccotti *et al.* [20, 21] for cross-laminated timber buildings. In this approach, a series of non-linear dynamic analyses are performed with the same input ground motion, scaled up in its acceleration amplitude until the structure fails [22]. The aim of this procedure is to find the acceleration level leading the building to attain the onset of yielding, defined as  $PGA_{el}$ , and the collapse condition, defined as  $PGA_{inel}$ . Such conditions are considered to be reached when the first spring in the model attains the elastic limit and the collapse, respectively.

The ratio between the aforementioned values gives an estimation of the behaviour factor of the structure, as expressed by Eqn (4).

$$q = \frac{PGA_{inel}}{PGA_{el}} \quad (4)$$

Two frame assemblies have been analysed: a simple portal frame (i) and a five-storey, three-bay frame (ii). Each model has been built in accordance with Figure 14(b). The two models are schematically displayed in Figure 17.

Both structures are made of Glulam beams connected by DVW-reinforced joints. They have been designed assuming a  $q$ -factor equal to 3. In the portal frame, the columns have a  $240 \times 700$  mm cross-section, while the beam has a double section of  $120 \times 700$  mm, with an applied gravity load of 9.4 kN/m. The fundamental vibration period is 0.45 s.

The portal frame hosts two dowel-type joints made with 10 tubes, placed with a radius of 220 mm from the centre of rotation, for a bending moment capacity of 292 kNm.

The five-storey, three-bay frame has the same glulam sections used for the portal frame, with a gravity load applied in the seismic combination of 30.3 kN/m on floors and 5.3 kN/m on roof. Its fundamental vibration period is 0.27 s.

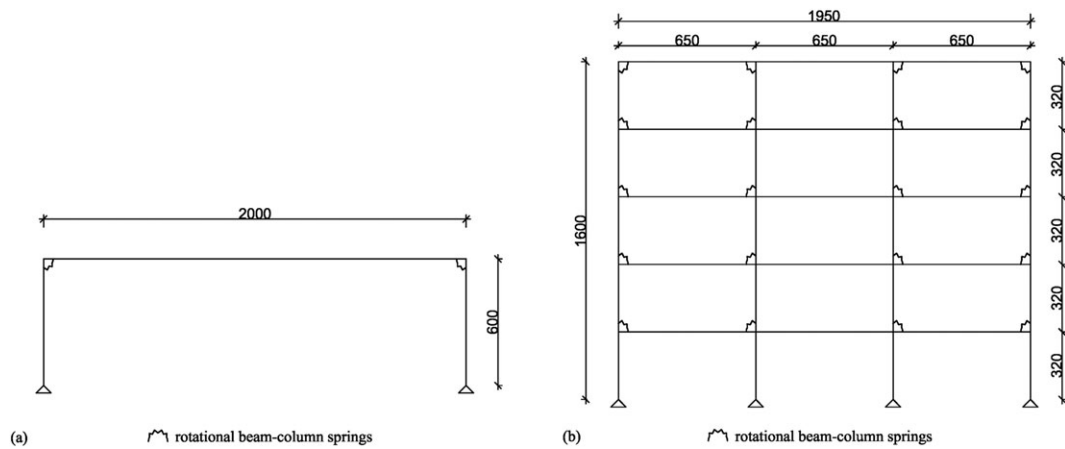


Figure 17. Portal (a) and five-storey, three-bay (b) frames, units in centimetres.

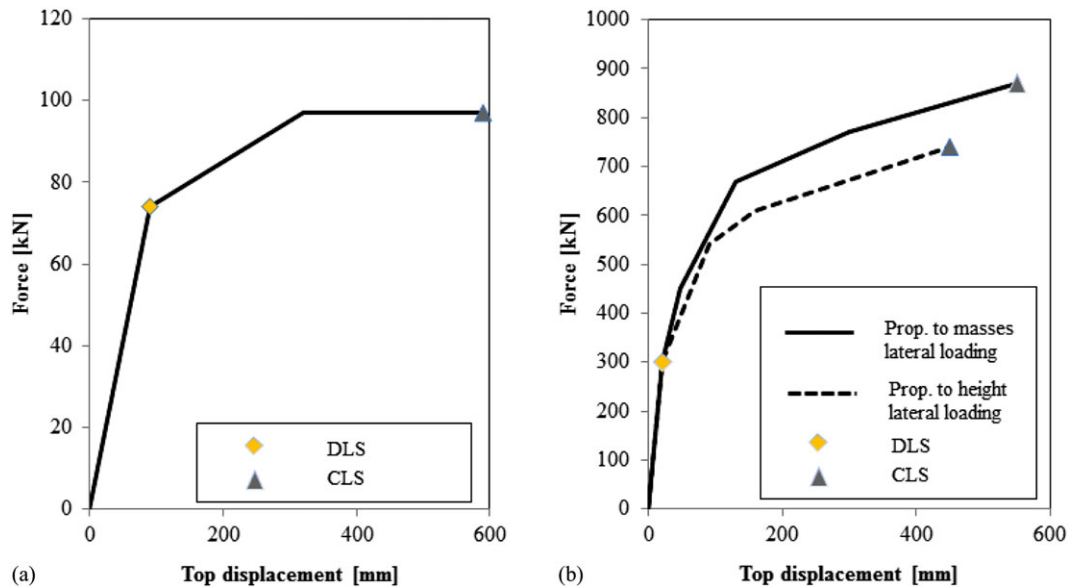


Figure 18. Results of pushover analyses for portal frame (left) and five-storey, three-bay frame (right), units in kilonewtons and millimetres.

The moment capacity of the 10-tube joints employed is 195 kNm, with a distance from the rotation centre of 213 mm. Such values have been obtained by hand calculations, as suggested by Leijten [2], and the cyclic behaviour has been taken from the experimental tests presented before.

Both frames are simply supported at their base. Before running the IDAs, a pushover analysis has been carried out on both frame assemblies with the aim to assess their load-carrying capacity. For the portal frame, after the gravity load is applied, a non-linear static analysis is performed, resulting in the capacity curve showed in Figure 18(a), with a maximum lateral load-carrying capacity of 95 kN. For the five-storey, three-bay frame, two lateral loads distributions have been used, one proportional to the floor masses and another proportional to the product of the floor masses by the storey heights. An average lateral load-carrying capacity in terms of base shear of 800 kN has been found, as displayed in Figure 18(b). On these curves, the damage limit state (DLS) and the collapse limit state (CLS) have been marked, which correspond to the attainment of the yield rotation and of the ultimate rotation in the first rotational spring, respectively. For such types of joints, yield rotation is generally low, because of the stiffness contribution of the DVW layers. For this reason, the interstorey drift limits for DLS given by the various design codes, such as FEMA-450 [23], are always complied with. Regarding the CLS, the ultimate rotations found in the experimental tests (Table 6) are much larger (more than 62 mrad vs 50 mrad) than the drift limits given by some design codes such as FEMA for CLS.

In order to perform an IDA, two sets of seven-recorded ground motions with their average elastic spectrum consistent in acceleration with a given design spectrum have been selected using the REXEL v3.5 software developed by Iervolino *et al.* [24]. The elastic design spectra used as a reference and evaluated according to Eurocode 8 [13] for Gemona, Italy, and Loppersum, the Netherlands, have been used as a base for selection. In both cases, it was assumed soil class type A. The upper and lower tolerances applied within the software REXEL are 10% in the period range from 0.1 to 2.0 s. For Gemona elastic spectrum, the seven natural records were taken from the Italian Accelerometric data base [25, 26], and a scale factor for accelerations less than 4 was applied. For Loppersum elastic spectrum, which has a PGA of 0.42 g, records were selected from the European Strong-motion Database [27], and the maximum scale factor was around 4.5. All the elastic spectra are displayed in Figure 19.

Incremental dynamic analyses have been performed using both seismic record sets, leading to the results displayed in Figure 20 in terms of  $q$ -factors versus PGA in  $m/s^2$ . The attainments of DLS and CLS have been marked for each curve presented.

As can be seen, the obtained values are scattered, because of the high influence of the frequency contents of the selected records on the analysed structures. This can be observed particularly in the five-storey, three-bay frame, where a maximum  $q$  factor of 31.9 has been computed, while for the portal frame, the values are less scattered. All the results are summarised in Table 7, from which the

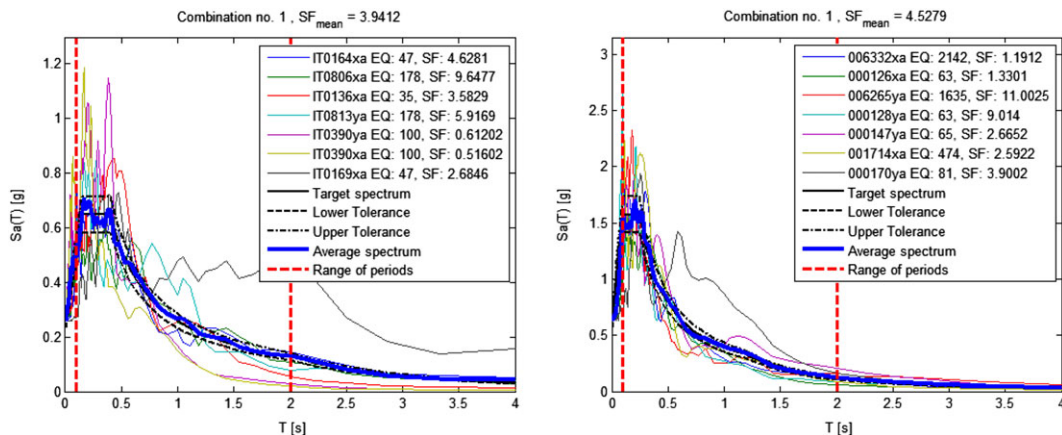


Figure 19. Spectra of the natural records selected to be consistent in acceleration with Gemona design spectrum, Italy (left) and with Loppersum, the Netherlands (right) and their average (in blue line), screenshots from REXEL v3.5 [24].



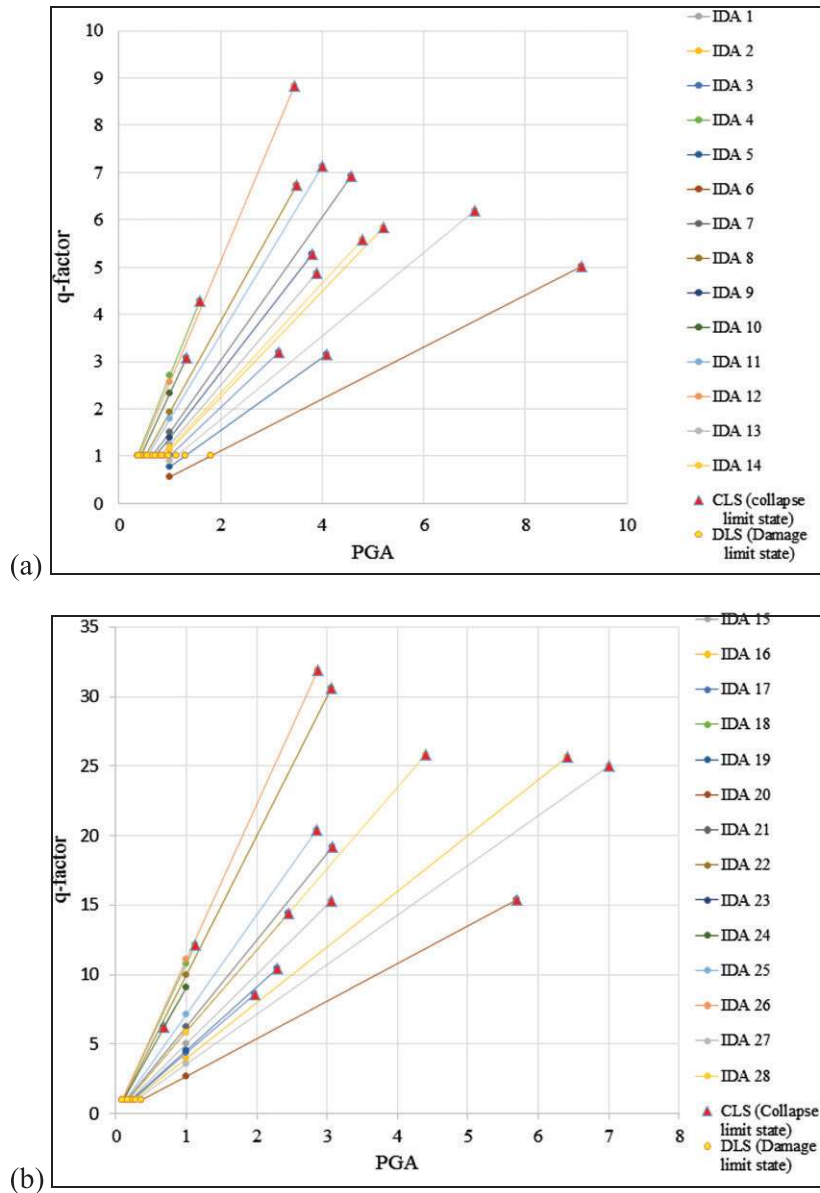


Figure 20. Behaviour factors versus PGA, in  $m/s^2$ , for the portal frame (a) and the five-storey, three-bay frame (b).

Table VII. Summary of the behaviour factors  $q$  obtained from incremental dynamic analyses.

Elastic spectrum	Portal frame			Five-storey, three-bay frame		
	Mean	Min.	Max.	Mean	Min.	Max.
Loppersum	4.8	3.2	6.9	15.2	8.6	25.7
Gemona	6.1	3.1	8.8	22.1	6.3	31.9
Average $q$ -factor	5.4	3.15	7.85	18.7	7.45	28.8

minimum behaviour factors of 3 and 6 can be assumed for the design of the portal frame and of the five-storey, three-bay frame, respectively. It should be noticed that the current version of Eurocode 8 prescribes a maximum value of the behaviour factor of 4 for hyperstatic portal frames with high-

dissipative joints. Based on the analyses carried out, such a value may be too high for portal frame and too conservative for multi-storey, multi-bay frames.

## 7. CONCLUSIONS

In this paper, the experimental programme carried out at Eindhoven University of Technology for investigating the cyclic behaviour of DVW-reinforced joints with expanded tube fasteners has been presented and critically discussed. Several specimens with different numbers and diameters of fasteners have been tested. Such a type of connection is particularly suitable for use in earthquake-prone areas because of its high-ductility ratio and energy dissipation capacity. The conducted experiments showed that high EVDR in the range 0.25 to 0.35 and large ductility ratios in the range 6 to 14 can be obtained for the connections with 18- and 35-mm-diameter tubes, respectively. According to Eurocode 8, the proposed connections can be classified as highly dissipative.

With the aim to investigate the seismic behaviour of entire moment-transmitting frames and to compute their behaviour factors, a portal frame and a five-storey, three-bay frame with DVW-reinforced joints have been first designed and then analysed under seismic actions.

High  $q$ -factors have been found: the minimum value is 3 and 6 for the portal frame and five-storey, three-bay frame, respectively. Such values are different from the value of 4 prescribed by Eurocode 8 for hyperstatic portal frames with highly dissipative connections. The presented analyses confirm the excellent ductile and dissipative behaviour of the dowel-type connections strengthened with DVW plates, making this technology very suitable for its use in seismic areas. The high  $q$ -factor values found are the direct consequence of the high ductility of the joints, which can undergo large rotations. Structural damage is limited thanks to the DWV layers, which allow the connection to concentrate all the damage on the steel dowels. At the end of the seismic event, the steel dowel can be replaced after recentering the connection. On the other hand, non-structural damage due to the large displacement achieved has to be limited or avoided with proper design considerations depending upon the type of partitions used and the destination of the building. For these reasons, from the damage mitigation standpoint, high  $q$ -factors might be carefully employed in structural design. In practical applications, the minimum  $q$ -factors found in this work can be used, carefully considering the damage in the rest of the structure (both in structural and non-structural components) by simply evaluating the rotation of joints at the chosen ductility level.

To draw final conclusions on the behaviour factor, different types of plane multi-storey, multi-bay frames will be analysed by varying the number of bays and storey involved in the simulation, with the aim to generalise the results found in this work. Furthermore, also three-dimensional frame structures will be analysed.

## ACKNOWLEDGEMENTS

The authors acknowledge the support of COST Action FP1004 for the short-term scientific mission of the first author, which made possible this work.

## REFERENCES

1. Johansen KW. Theory of timber connections. *International Association for Bridge and Structural Engineering* 1949; **9**:249–262.
2. Leijten AJM. *Densified veneer wood reinforced timber connections with expanded tube fasteners, Doctoral Thesis*. Delft University Press: the Netherlands, 1998.
3. Rodd PD, Leijten AJM. High-performance dowel-type joints for timber structures. *Progress in Structural Engineering and Materials* 2003; **5**(2):77–89.
4. Leijten AJM, Brandon D. Advances in moment transferring DVW reinforced timber connections: analysis and experimental verification, part 1. *Construction and Building Materials* 2013; **43**:614–622. DOI:10.1016/j.conbuildmat.2013.03.020.
5. Brandon D, Leijten AJM. Advances in moment transferring DVW reinforced timber connections: numerical analyses and verification, part 2. *Construction and Building Materials* 2014; **56**:32–43. DOI:10.1016/j.conbuildmat.2014.01.026.

6. Leijten AJM, Ruxton S, Prion H, Lam F. Reversed-cyclic behavior of a novel heavy timber tube connection. *ASCE Journal of Structural Engineering* 2006; **132**(8):1314–1319.
7. Jorissen A. Double shear timber connections with dowel type fasteners. *HERON* 1999; **44**(3):163–186.
8. Blass HJ, Bienhaus A, Krämer V. (2001) Effective bending capacity of dowel-type fasteners. *Proceedings of PRO 22 – International RILEM Symposium on Joints in Timber Structures*, 71–80.
9. Uibel T, Blass HJ. (2006) Load carrying capacity of joints with dowel type fasteners in solid wood panels. *Proceedings of CIB Meeting 39*, August 2006, Florence, Italy.
10. Dias AMPG, Lopes SMR, Van De Kuilen JWG, Cruz HMP. Load-carrying capacity of timber–concrete joints with dowel-type fasteners. *Journal of Structural Engineering* 2007; **133**(5):720–727.
11. Rinaldin G, Fragiaco M. A component approach for the hysteretic behaviour of connections in cross-laminated wooden structures. *Earthquake Engineering and Structural Dynamics* 2013; **42**:1885–2042 Wiley Online Library. DOI:10.1002/eqe.2310.
12. Rinaldin G, Fragiaco M. Non-linear simulation of shaking-table tests on 3- and 7- storey X-Lam timber buildings. *Engineering Structures* 2016; **2016**(113):133–148. DOI:10.1016/j.engstruct.2016.01.055.
13. CEN (2005) Eurocode 8. Design of structures for earthquake resistance – Part 1, General rules, seismic actions and rules for buildings. EN 1998–1:2005.
14. Wrzesniak D, Amadio C, Rinaldin G, Fragiaco M. (2013) Non-linear cyclic modelling of moment-resisting timber frames, *Proceedings of ANIDIS 2013*, Padua, Italy.
15. Wrzesniak D, Rinaldin G, Fragiaco M, Amadio C. (2014) Proposal for the q-factor of moment-resisting timber frames with high ductility dowel connectors. *Proceedings of the CIB W18 Meeting*, 37, August 2014.
16. EN 12512: 2002 Timber Structures – test methods – cyclic testing of joints made with mechanical fasteners.
17. EN 26891:1991 Timber structures – joints made with mechanical fasteners – general principles for the determination of strength and deformation characteristics.
18. Rinaldin G So.ph.i. program version 4.55, Internet site: <http://giovanni.rinaldin.org/>, 2011–2015.
19. EN 14358:2006 Timber structures – Calculation of characteristic 5-percentile values and acceptance criteria for a sample.
20. Ceccotti A, Karacabeyli E. (1998) Seismic performance of moment resisting timber frames, *Proceedings of World Conference on Timber Engineering, WCTE 2008*, Lausanne, Switzerland.
21. Ceccotti A, Follasa M, Lauriola MP, Sandhaas C, Minowa C, Kawai N, Yasumura M. Which seismic behaviour factor for multi-storey buildings made of cross-laminated wooden panels. *Meeting 39 of the Working Commission W18-Timber Structures*. CIB: Florence (Italy) August 28–31, 2006.
22. Vamvatsikos D, Cornell CA. Incremental dynamic analysis. *Earthquake Engineering & Structural Dynamics* 2002; **31**(3):491–514.
23. Building seismic safety council. The 2003 NEHRP recommended provisions for new buildings and other structures Part 1: Provisions (FEMA 450).
24. Iervolino I, Galasso C, Cosenza E. REXEL: computer aided record selection for code-based seismic structural analysis. *Bulletin of Earthquake Engineering* 2010; **8**:339–362. DOI:10.1007/s10518-009-9146-1.
25. Luzi L, Hailemikael S, Bindi D, Pacor F, Mele F, Sabetta F. ITACA (ITalian ACcelerometric Archive): a web portal for the dissemination of Italian strong-motion data. *Seismological Research Letters* 2008; **79**(5):716–722. DOI:10.1785/gssrl.79.5.716.
26. Pacor F, Paolucci R, Luzi L, Sabetta F, Spinelli A, Gorini A, Nicoletti M, Marcucci S, Filippi L, Dolce M. Overview of the Italian strong motion database ITACA 1.0. *Bulletin of Earthquake Engineering* 2011; **9**(6):1723–1739. DOI:10.1007/s10518-011-9327-6.
27. European strong-motion database, n d *Internet site*: <http://www.isesd.hi.is/>.
28. Kasal B, Heiduschke A, Haller P. (2002) Fibre-reinforced beam-to-column connections for seismic applications. *Proceedings of CIB-W18*, paper 37-7-12.
29. Schreyer AC. (2002) Cyclic behaviour of slender dowel-type fasteners in wood–steel connections. PhD-thesis, Wiesbaden: Fachhochschule Wiesbaden Germany.
30. Rinaldin G, Fragiaco M. Non-linear simulation of shaking-table tests on 3- and 7-storey X-Lam timber buildings. *Engineering Structures* 2016; **113**:133–148. DOI:10.1016/j.engstruct.2016.01.055.
31. Bedon C, Rinaldin G, Fragiaco M. Non-linear modelling of the in-plane seismic behaviour of timber *Blockhaus* log-walls. *Engineering Structures* 2015; **91**:112–124. DOI:10.1016/j.engstruct.2015.03.002.
32. Rinaldin G, Herve Poh'sie G, Amadio C, Fragiaco M. Modelling the seismic behaviour of light-frame timber structures. *Ingegneria Sismica, International Journal of Earthquake Engineering*, **4**:82–98, December 01, 2013, Italy.